A new type of DNA "light switch": a dual photochemical sensor and metalating agent for duplex and G-quadruplex DNA

Erin Wachter, Brock S. Howerton, Emily C. Hall, Sean Parkin, and Edith C. Glazer*

University of Kentucky, Lexington, KY 40506

Supporting Information

1. Instrumentation
2. Materials
3. Synthesis
4. Crystallography
5. DNA Gel Electrophoresis
6. DNA Binding Studies
7. Photoejection Kinetics
8. Luminescence Studies
9. Analysis of Covalent Adduct Formation by HPLC
10. Additional Figures and Tables:

Figure S1. ESI-MS showing the ejection products in the presence of CT DNA.
Figure S2. HPLC chromatograms show the covalent attachment of **2** to the 15-mer oligonucleotide A following light activation.
Figure S3. HPLC chromatogram of **2**.
Figure S4. Photoejection of **2** in the presence of the 15-mer oligonucleotide A.
Figure S5. Photoejection of **2** in CH_2Cl_2.
Figure S6. Photoejection of **2** +/- $Bu_4N^+Cl^-$ in CH_2Cl_2
Figure S7. Final spectra of **2** after photoejection in CH_3CN and CH_2Cl_2:CH_3CN (99:1).
Figure S8. Photoejection of **2** in H_2O.
Figure S9. Photoejection of **2** in D_2O.
Figure S10. Photoejection of **2** in the presence of G-quadruplex DNA.
Figure S11. Photoejection of **2** in the presence of bovine serum albumin (BSA).
Figure S12. Agarose gel electrophoresis of **1** and **2** with pUC19 DNA.
Figure S13. Emission spectra of **1** in pure solvents.
Figure S14. Emission spectra of **1** in the presence of DNA under different conditions.
Table S1. Photophysical data for compound **1**.
Figure S15. Ellipsoid plot of **1**.
Table S2. Selected bond lengths, bond angles, and torsion angles for compound **1**.
Figure S16. Ellipsoid plot of **2**.
Table S3. Selected bond lengths, bond angles, and torsion angles for compound **2**.

11. References

1. Instrumentation:

All ^{1}H NMR were obtained on a Varian Mercury spectrometer (400 MHz) and chemical shifts reported relative to the residual solvent peak in CD_3CN (δ 1.94) or $CDCl_3$ (δ 7.24). The ^{13}C chemical shifts are reported relative to the residual solvent peak in CD_3CN (δ 1.39). Electrospray ionization (ESI) mass spectra were obtained on a Varian 1200L mass spectrometer at the University of Kentucky Environmental Research Training Laboratory (ERTL). Absorption spectra were obtained on an Agilent 8453 Diode Array UV/Vis Spectrophotometer and a Cary 60 UV/Vis Spectrophotometer. Photoejection experiments were performed using a Dell 200 Watt 1410X projector. An Edmund Optics filter (Item Number NT43-941) was used to cut-off wavelengths < 400 nm. Photoejection experiments were performed in a 1 cm path length quartz cuvette placed 30 cm from the projector. Kinetics were fit using the equation for a single exponential with the Prism software package. Luminescence spectra were obtained on a Horiba Jobin Yvon Fluorolog-3 Spectrofluorometer equipped with a Hamamatsu type R928P photomultiplier tube.

HPLC Analysis:
Samples were injected on an Agilent 1100 Series HPLC equipped with a model G1311A quaternary pump, G1315B UV diode array detector and Chemstation software version B.01.03. Chromatographic conditions for ruthenium complexes were optimized on a Column Technologies Inc. C18 column (120 Å, 250 mm x 4.6 mm, 5 µm) fitted with a Phenonmenex C18 (4 mm x 3 mm) guard column. Conditions were optimized for DNA analysis on a Grace Davison Discovery Sciences (Vydac 218TP C18 5µ) C18 column (300 Å, 250 mm x 4.6 mm, 5 µm) fitted with a Phenonmenex C18 (4 mm x 3 mm) guard column. Injection volumes of 5 µL were used for all samples. The detection wavelength was 280 nm. The mobile phases were composed of 0.1% formic acid in dH_2O and 0.1% formic acid in HPLC grade acetonitrile (Pharmco-Aaper). The gradient used for all samples is shown in the table below.

Time (min)	0.1% formic acid in dH_2O	0.1% formic acid in CH_3CN
0	98	2
2	95	5
5	70	30
15	70	30
20	40	60
30	5	95
35	98	2
40	98	2

2. Materials:

Chemicals used for synthesis were purchased from suppliers and used without further purification. Calf thymus (CT) DNA was purchased from Sigma-Aldrich, re-suspended in buffer (50 mM NaCl, 5 mM Tris buffer, pH 7.0) and sonicated (bath sonicator for 40 min followed by 10–15 1 sec pulses with a Branson Sonifier 250 (duty cycle = 90% and output control = 2) to provide shorter strands for these studies. The 15-mer oligonucleotide A was purchased from Integrated DNA Technologies and the G-quadruplex sequence was purchased from Eurofins, re-suspended, and annealed prior to use. The forward sequence for the 15-mer oligonucleotide A is 5'-CCT-CTC-TGG-TTC-TTC-3' and the reverse sequence is 5'-GAA-GAA-CCA-GAG-AGG-3'. The 15-mer oligonucleotide was re-suspended in dH_2O and annealed by heating at 90 °C for 5 min then cooling slowly to ambient temperature and stored at -20 °C. The G-quadruplex sequence is 5'-

[AGGG(TTAGGG)$_3$]-3'. The G-quadruplex was re-suspended in buffer (10 mM potassium phosphate, 100 mM KCl, pH 7.0) and annealed by heating at 90 °C for 5 min then cooling slowly to ambient temperature, followed by incubation at 4 °C overnight, as previously reported.[1]

3. Synthesis:

Dipyrido[3.2-a:2',3'-c]phenazine (**dppz**) and Ru(bpy)$_2$dppz (**1**) were prepared by literature methods.[2,3]

3,6-Dimethyl-dipyrido[3,2-*a*:2',3'-*c*]phenazine (**dmdppz**):
Dimethyl-dipyrido[3,2-*a*:2',3'-*c*]phenazine was prepared by modification of literature methods using 2,9-dimethylphendione (**note the different numbering system; this is equivalent to the 3,6 positions on dppz**) instead of the starting material phendione.[2] Yield: 0.9 g (65 %). ^{1}H NMR ($CDCl_3$, 400 MHz): δ 9.50 (d, J = 8.2 Hz, 2H), 8.31 (d, J = 6.6 Hz, 2H), 7.81 (d, J = 6.5, 2H), 7.63 (d, J = 8.2 Hz, 2H), 2.97 (s, 6H). ESI MS calcd for $C_{20}H_{14}N_4$ [M] 310.12; found 311 $[MH]^+$. ^{13}C NMR was not obtained due to poor solubility of the free ligand.

Ru(bpy)$_2$dmdppz **(2):**
$Ru(bpy)_2Cl_2 \cdot 2H_2O$ (501 mg, 0.963 mmol) and 3, 6-dimethyl-dipyrido[3,2-*a*:2',3'-*c*]phenazine (328 mg, 1.057 mmol) were added to 16 mL of degassed ethylene glycol in a 38 mL pressure tube. The mixture was heated at 150 °C with stirring and protected from light. After 16 hours the red solution was cooled to room temperature and poured into 50 mL of distilled water. Addition of a saturated aqueous KPF_6 solution produced a deep red precipitate that was collected by vacuum filtration and washed with dH_2O (50 mL) and diethyl ether (50 mL). Purification of the solid was carried out by flash chromatography on SiO_2. Elution with saturated aq. $KNO_3/H_2O/CH_3CN$ (5/15/80) gave the pure complex. After column purification the complex as the NO_3^- salt was dissolved in a minimal volume of water, and a saturated aq. solution of KPF_6 was added. The complex was extracted into CH_2Cl_2 and the solvent removed under reduced pressure to give a deep red solid. Yield: 361 mg (37%). ^{1}H NMR (CD_3CN, 400 MHz): δ 9.65 (d, J = 8.2 Hz, 2H), 8.52 (d, J = 8.4 Hz, 2H), 8.48-8.44 (m, 4H), 8.13-8.10 (m, 2H), 8.07-7.98 (m, 4H), 7.85 (d, J = 5.7 Hz, 2H), 7.79 (d, J = 8.3 Hz, 2H), 7.72 (d, J = 5.7 Hz, 2H), 7.32-7.27 (m, 4H), 2.09 (s, 6H); ^{13}C NMR (CD_3CN, 100 MHz): δ 169.70, 158.66, 158.50, 154.15, 152.98, 152.74, 144.10, 140.44, 139.06, 138.86, 135.34, 133.30, 130.64, 129.66, 129.62, 128.56, 128.47, 125.63, 125.54, 26.47, 20C; ESI MS calcd for $C_{40}H_{30}N_8Ru$ $[M]^{2+}$ PF_6^- 869.12, $[M]^+$ 724.16, $[M]^{2+}$ 362.08; found 869.1 $[M]^{2+}$ PF_6^-, 723.3 $[M]^+$, 362.1 $[M]^{2+}$. Purity by HPLC: 97% by area. UV/Vis (CH_3CN): λ_{max} nm (ε $M^{-1}cm^{-1}$) 284 (88,900), 325 (23,600), 352 (18,900), 450 (14,100).

Counterion Exchange:

Compounds **1** and **2** were converted to the Cl^- salt prior to experiments. The PF_6^- salt of each complex was dissolved in a minimal volume of acetone (1–2 mL), followed by the addition of a solution of t-butyl ammonium chloride (1 g dissolved in 5 mL of acetone) producing a precipitate that was filtered through glass wool, washed with acetone (50 mL) and eluted with acetonitrile. The solvent was removed under reduced pressure to give the pure complex.

4. Crystallography:

As compound **2** is unstable with respect to light, all crystal manipulations requiring exposure to light were conducted as rapidly as possible. To this end, the crystal(s) were plunged directly into liquid nitrogen and mounted using cryo-tongs[4] initially developed for crystals of biological macromolecules.

Single crystals of compounds **1** and **2** were grown by slow evaporation of methylene chloride in diethyl ether, mounted in inert oil and transferred to the cold gas stream of the diffractometer. X-ray diffraction data were collected at 90.0(2) K on a Bruker-Nonius X8 Proteum diffractometer with graded-multilayer focused CuK(α) x-rays. Raw data were integrated, scaled, merged and corrected for Lorentz-polarization effects using the APEX2 package.[5] Corrections for absorption were applied using SADABS[6] and XABS2.[6] The structure was solved by direct methods (SHELXS-97[6]) and difference Fourier (SHELXL-97[7]). Refinement was carried out against F^2 by weighted full-matrix least-squares (SHELXL-97[7]), and assessed with the aid of an R-tensor.[8] Hydrogen atoms were found in difference maps but subsequently placed at calculated positions and refined using a riding model. Non-hydrogen atoms were refined with anisotropic displacement parameters. Atomic scattering factors were taken from the International Tables for Crystallography.[9] Crystal data and relevant details of the structure determinations are summarized below and selected geometrical parameters are given in Table S1 and S2.

Crystal data compound 1: $C_{43.18}H_{37.25}C_{12.86}F_{12}N_8O_{0.94}P_2Ru$, M = 1175.67, triclinic, space group Pī, a = 17.115(2) Å, b = 17.367(2) Å, c = 17.373(2) Å, V = 4863.9(10) Å^3, ρ_{calcd} = 1.606 Mg/m^3, λ = 1.54178 Å, T = 90.0(2) K, Z = 4, 62989 reflections measures, 17033 unique (R_{int} = 0.0656), and the final R1 = 0.0817 [I >2σ(I)].

Crystal data compound 2: $C_{41}H_{32}F_{12}N_8Cl_2P_2Ru$, M = 1089.40, monoclinic, space group P 2_1/c, a = 14.5892(4) Å, b = 38.7805(10) Å, c = 15.4066(4) Å, V = 8505.6(4) Å^3, ρ_{calcd} = 1.702 Mg/m^3, λ = 1.54178 Å, T = 150(2) K, Z = 8, 99883 reflections measured, 15055 unique (R_{int} = 0.0459), and the final R1 = 0.0513 [I>2σ(I)].

5. DNA Gel Electrophoresis:

Complex **1** and **2** were serially diluted 1:2 to give final concentrations of 0, 7.8, 15.6, 31.3, 62.5, 125, 250, and 500 μM of compound. The compound in dose response was equilibrated with 40 μg/mL of pUC19 plasmid in 10 mM phosphate buffer, pH 7.4, and incubated overnight prior to gel electrophoresis. DNA control samples were prepared as previously reported.[10]

Gel Electrophoresis: DNA samples were resolved on a 1% agarose gel in 1x Tris-Acetate (TA) buffer, with 0.3 μg of plasmid loaded per lane. The samples were run for 120 min at 100 mV followed by staining the gel with a solution of 500 ng/mL Ethidium Bromide in 1x TA buffer for 40 min. The gels were destained in 1x TA buffer for 30 min and digitally imaged with the BioRad ChemiDoc System.

6. DNA Binding Studies:

20 μM Ru^{II} complexes in buffer (50 mM NaCl, 5 mM Tris, pH 7.0) were titrated with CT DNA with ratio of 0 to 4 base pairs per ruthenium. The maximum change was obtained at a 2:1 [bp]:[Ru] ratio. The change in extinction coefficient was plotted versus CT DNA concentration and K_b values were determined using Prism software.[11]

7. Photoejection Kinetics:

Pure solvents: Photoejection studies were conducted in 3 mL of CH_2Cl_2, DMF, H_2O, and D_2O in a quartz cuvette with a final concentration of 18–20 μM compound **2**. The sample was protected from ambient light and irradiated with light from a Dell 1410X 200 W projector using a blue cut-off filter (> 400 nm light

passes). Scans were taken at appropriate time points to monitor ligand ejection. The normalized change in extinction coefficient was plotted against time to determine the half-life of ejection using Prism software.

Biological Molecules:

A) Compound **2** was added to CT DNA (50 mM NaCl, 5 mM Tris, pH 7.0) in a 400 μL quartz cuvette to give final concentrations of 200 μM nucleotides and 20 μM **2**; a 10:1 [Nu]:[Ru] ratio. This experiment was repeated for 15-mer oligonucleotide A under the same conditions.

B) Compound **2** was added to the annealed G-quadruplex (10 mM potassium phosphate, 100 mM KCl, pH 7.0) to give final concentrations of 40 μM nucleotides and 20 μM **2**; a 2:1 [Nu]:[Ru] ratio.

C) Compound **2** was added to BSA (50 mM NaCl, 5 mM Tris, pH 7.0) to give final concentrations of 20 μM BSA and 20 μM **2**, a 1:1 [BSA]:[Ru].

Spectra for each condition above were obtained and plotted in the same manner as the pure solvents.

8. Luminescence Studies:

Luminescence spectra (λ_{ex} = 440 nm) were collected in CH_2Cl_2, DMF, H_2O, and D_2O with 5 μM compound **1**. Luminescence spectra were also obtained for each DNA condition described above with 5 μM compound **1** (λ_{ex} = 440 nm).

9. Analysis of Covalent Adduct Formation by HPLC:

The 15-mer oligonucleotide A (250 μM nucleotide) was incubated with 500 μM **2** in the dark or was irradiated with >400 nm light for 3 hours. Samples were then incubated at 37 ^{o}C overnight before HPLC analysis. The DNA duplex in the absence of compound was run as a reference. Chromatography was performed using the method described above using a Grace Davison Discovery Science (Vydac 218TP C18 5μ) C18 column.

10. Additional Figures.

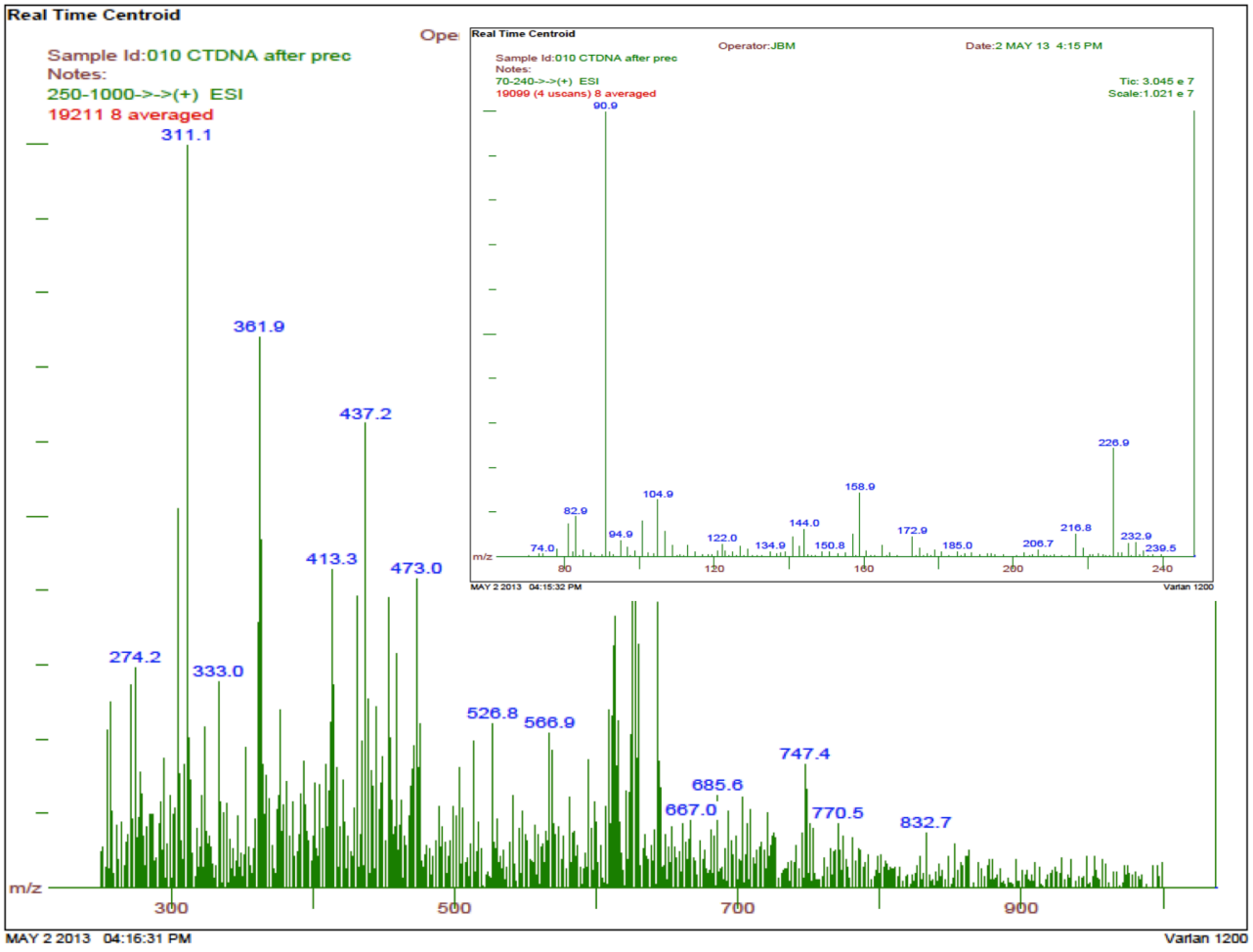

Figure S1. ESI-MS showing the ejection products in the presence of CT DNA. Dmdppz ($C_{20}H_{14}N_4$) [M] = 310.12, found 311.1 $[MH]^+$. Inset shows no 2,2'-bipyridine ($C_{10}H_8N_2$) was found ([M] = 156.07).

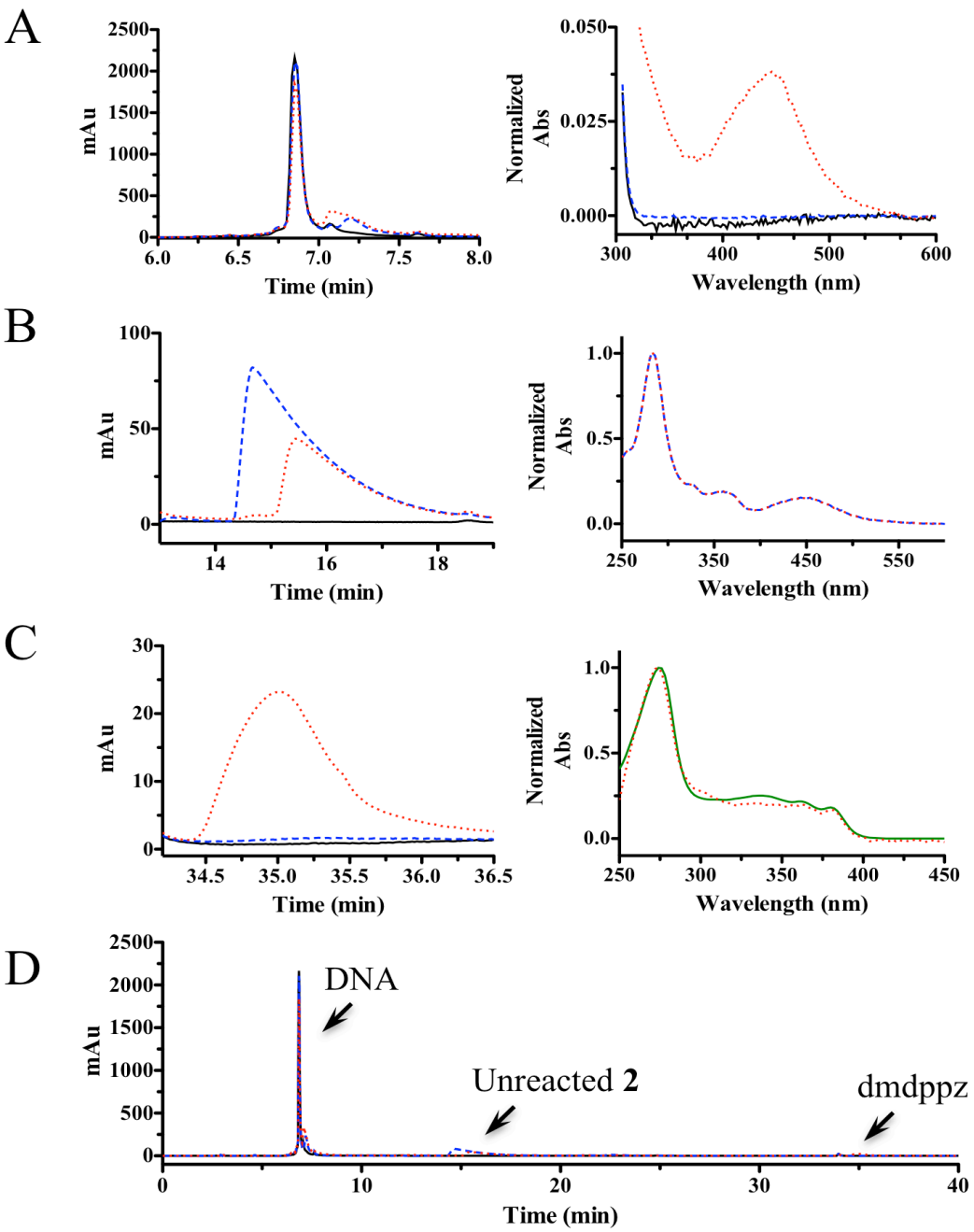

Figure S2. HPLC chromatograms show the covalent attachment of **2** to the 15-mer oligonucleotide A following light activation. For all chromatograms and absorption spectra: DNA only (black); DNA:**2** in the absence of light (blue); DNA:**2** in the presence of light (red); dmdppz ligand (green). A. Left: Expansion overlay of chromatograms of DNA-containing peaks. The shift in retention when incubated with **2** in the dark and light is likely due to a perturbation of DNA structure by **2**. Right: UV/Vis spectra of peaks from 7–7.5 min. demonstrates that Ru^{II} is only retained with the DNA when the sample is light-activated. B. Left: Elution of unreacted **2**; the area decreases following light activation as the compound is converted to the active, DNA reactive form. Right: UV/Vis spectra of peaks from 14–18 min. show the absorption profile of **2**. C. Left: Elution of ejected dmdppz only upon light activation of **2** with DNA. Right: UV/Vis spectra of the peak at 35 min. show pure dmdppz and ejected dmdppz. D. Overlay of full HPLC chromatograms.

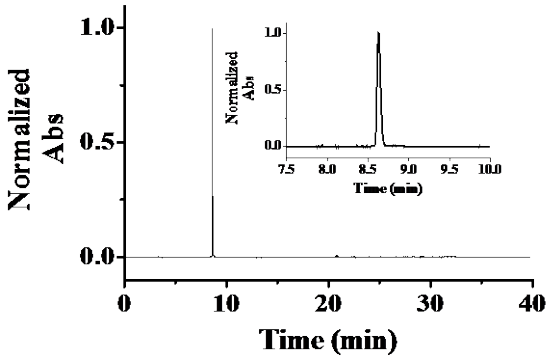

Figure S3. HPLC chromatogram of **2.** Inset displays an expansion of the peak. Purity by HPLC: 97 % by area. Note: sample run on a Column Technologies Inc. C18 column.

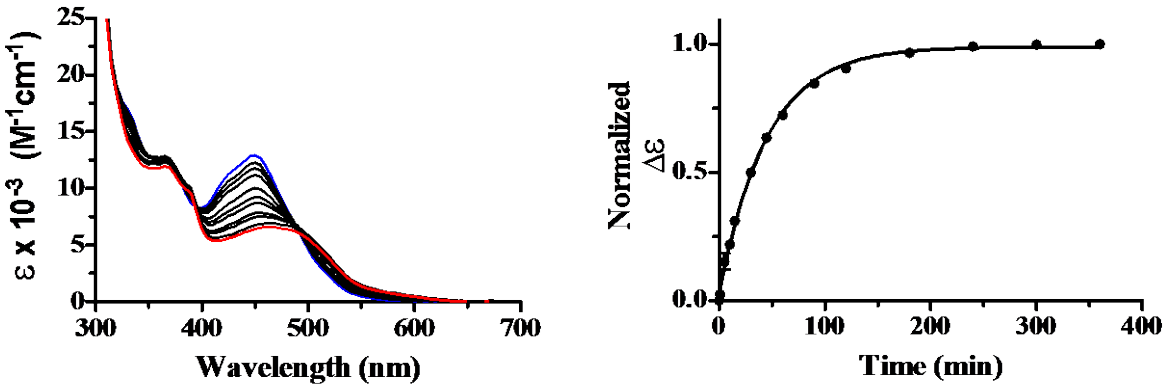

Figure S4. Photoejection of **2** in the presence of the 15-mer oligonucleotide A (50 mM NaCl, 5 mM Tris, pH 7.0) at a 1:10 [Ru]:[Nu] ratio. The difference in extinction coefficient (Δε 510-450 nm) was fit to a mono-exponential decay function using Prism software to obtain the half-life of ligand ejection. $t_{1/2}$ = 31.3 ± 0.5 min.

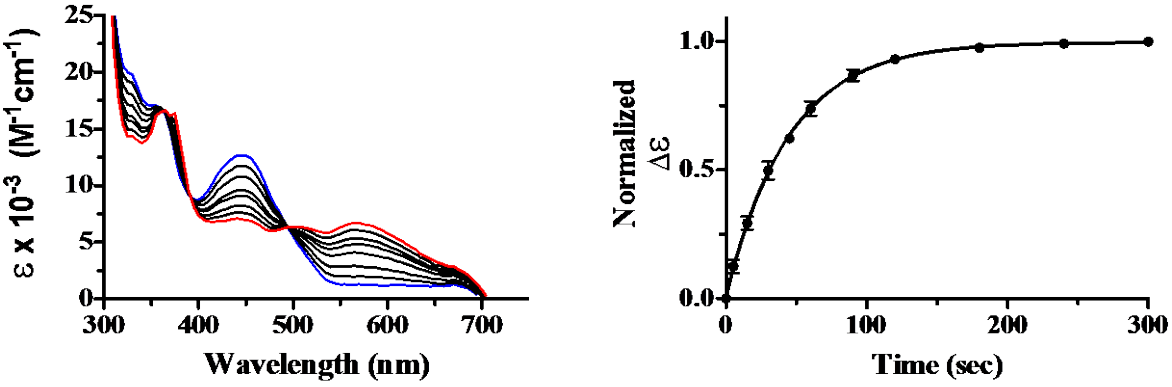

Figure S5. Photoejection of **2** in CH_2Cl_2. The difference in extinction coefficient (Δε 550-450 nm) was fit to a mono-exponential decay function using Prism software to obtain the half-life of ligand ejection. $t_{1/2}$ = 0.50 ± 0.05 min.

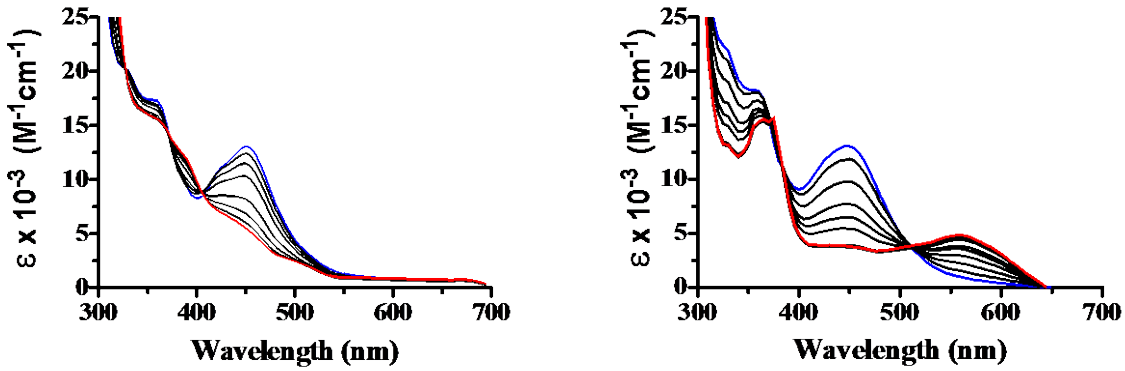

Figure S6. Photoejection of **2** +/- $Bu_4N^+Cl^-$ in CH_2Cl_2. Compound **2** (with 2 PF_6^- counter-ions) was photoejected without (left) and with (right) $Bu_4N^+Cl^-$ (10-fold excess). The addition of a Cl^- source provides evidence that the Cl^- acts as a ligand upon photoejection, and the final UV/Vis absorbance profile is dependent on the identity of the incoming ligand in solution.

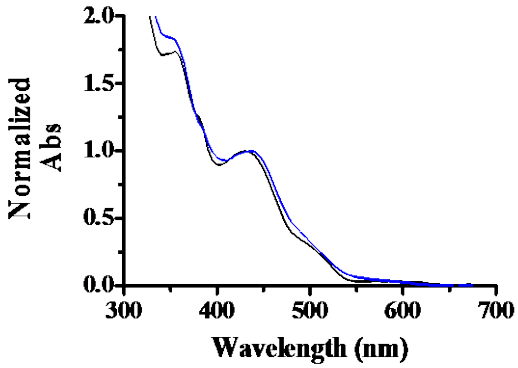

Figure S7. Final spectra of **2** after photoejection in CH_3CN and CH_2Cl_2:CH_3CN (99:1). Comparison of photoejection final absorbance spectra of **2** with 2 PF_6^- counter-ions in CH_3CN (black) and in CH_2Cl_2 with 1% CH_3CN (blue). Photoejection with 1% CH_3CN produces a final UV/Vis spectrum equivalent to that of $Ru(bpy)_2(CH_3CN)_2$.[12] (Note: some absorption due to the liberated dmdppz ligand is observed.)

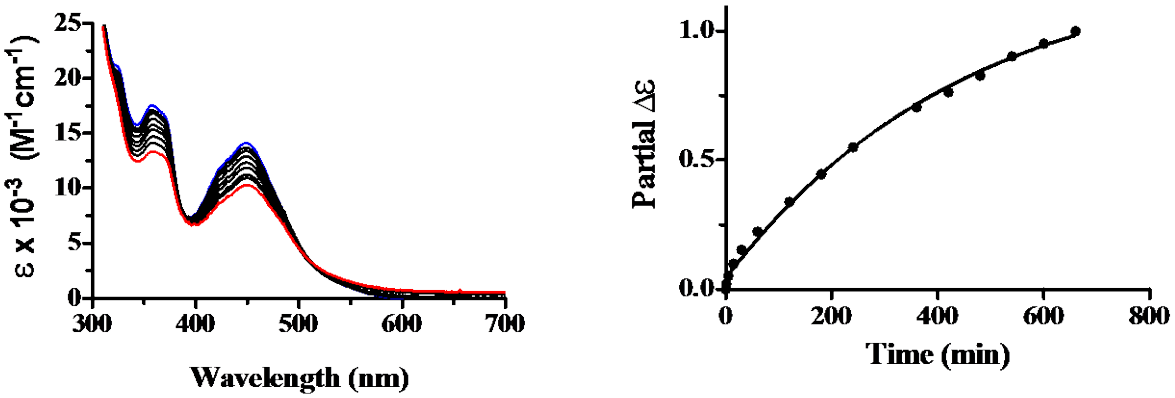

Figure S8. Photoejection of **2** in H_2O. The partial change in extinction coefficient at 450 nm was fit to a mono-exponential decay function using Prism software. The photoejection was incomplete after the 11-hour reaction time.

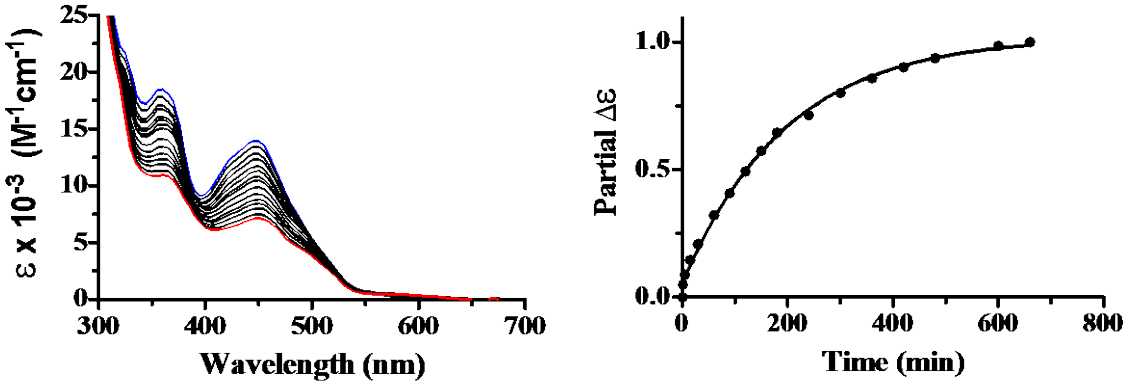

Figure S9. Photoejection of **2** in D_2O. The partial change in extinction coefficient at 450 nm was fit to a mono-exponential decay function using Prism software to obtain the half-life of ligand ejection. $t_{1/2}$ = 140 ± 11 min. Note: the reaction did not go to completion.

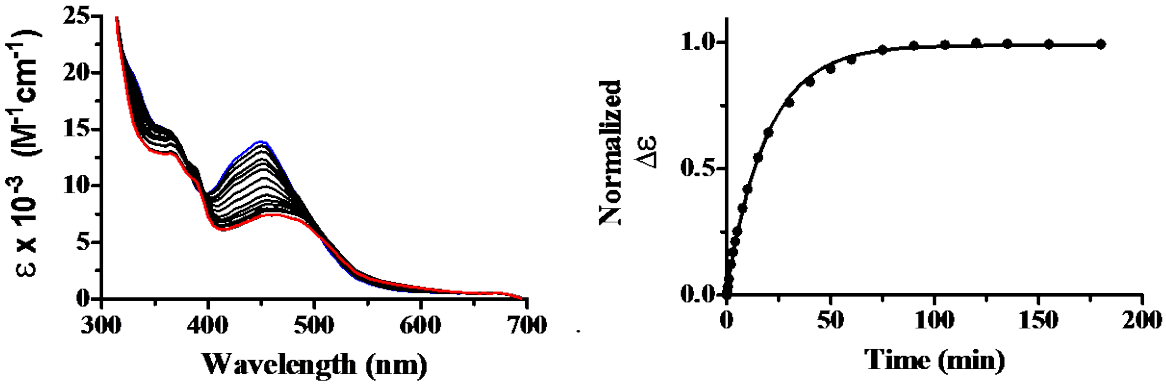

Figure S10. Photoejection of **2** in the presence of G-quadruplex DNA (10 mM KH_2PO_4–K_2HPO_4, 100 mM KCl, pH 7.0) at a 1:2 [Ru]:[Nu] ratio. The difference in extinction coefficient (Δε 550-450 nm) was fit to a mono-exponential decay function using Prism software to obtain the half-life of ligand ejection. $t_{1/2}$ = 13.5 ± 0.1 min.

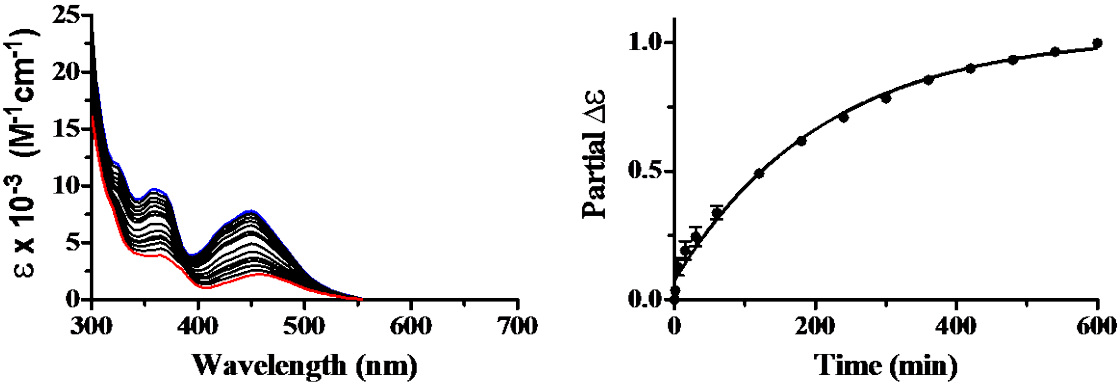

Figure S11. Photoejection of **2** in the presence of bovine serum albumin (BSA). The change in extinction coefficient at 450 nm was fit to a mono-exponential decay function using Prism software to obtain the half-life of ligand ejection. $t_{1/2}$ = 146 ± 8 min. Note: the reaction did not go to completion.

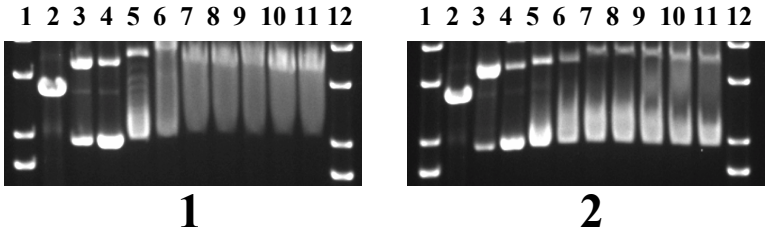

Figure S12. Agarose gel electrophoresis of **1** and **2** incubated with 40 μg/mL pUC19 plasmid (protected from light) showing intercalation at concentrations as low as 7.8 μM. Lane 1: DNA Ladder; Lane 2: EcoR1; Lane 3: $Cu(OP)_2$; Lane 4: 0 μM; Lane 5: 7.8 μM; Lane 6: 15.6 μM; Lane 7: 31.3 μM; Lane 8: 62.5 μM; Lane 9: 125 μM; Lane 10: 250 μM; Lane 11: 500 μM; Lane 12: DNA Ladder. EcoR1 and $Cu(OP)_2$ are used as controls for linear and relaxed circular DNA, respectively.

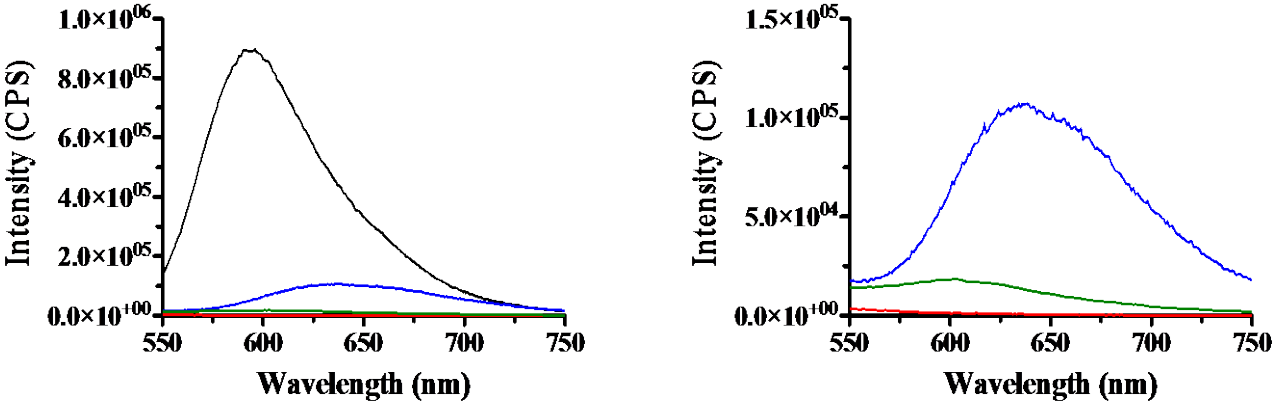

Figure S13. Uncorrected emission spectra of **1** (5 μM) in pure solvents. Left: the emission observed with CH_2Cl_2 (black), DMF (blue), D_2O (green) and H_2O (red); Right: data in CH_2Cl_2 is excluded to show the slight emission in D_2O and absence of emission in H_2O.

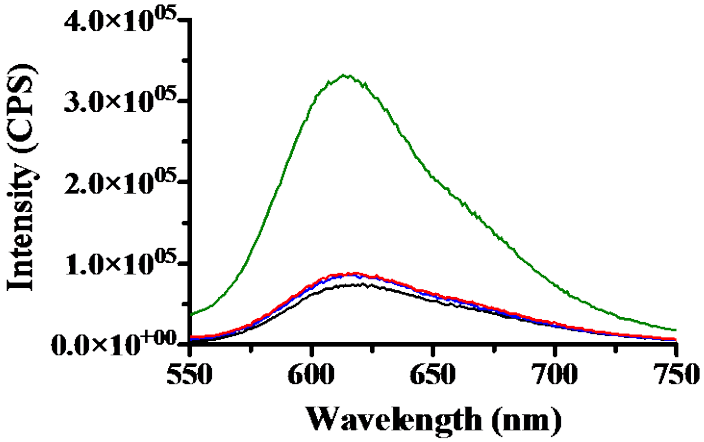

Figure S14. Uncorrected emission spectra of **1** with DNA under different conditions. Black: 1:10 [Ru]:[Nu] CT DNA (50 mM NaCl, 5 mM Tris, pH 7.0); Blue: 1:50 [Ru]:[Nu] CT DNA (5 mM phosphate, pH 7.0) with 2 mM $MgCl_2$; Red: 1:10 [Ru]:[Nu] 15-mer oligonucleotide A (50 mM NaCl, 5 mM Tris, pH 7.0); Green: 1:2 [Ru]:[Nu] G-quadruplex (10 mM KH_2PO_4–K_2HPO_4, 100 mM KCl, pH 7.0). Note: blue and red lines overlay.

Table S1. Photophysical data for compound **1**.

	Uncorrected λ_{max}(nm)	Corrected λ_{max}(nm)	Literature λ_{max}(nm)
H_2O	No emission	No emission	-
D_2O	605[a]	626[a]	-
CH_2Cl_2	596	601	592[b]
DMF	638	670	625[b]
CT DNA	619	636	632[c]
15-mer oligonucleotide A	615	637	-
G-quadruplex folded	613	637	-
BSA	No emission	No emission	-

[a] Negligible emission (see Figure S13). [b] See reference 13. [c] See reference 14. Corrected with Origin software using the Horiba S detector correction file.

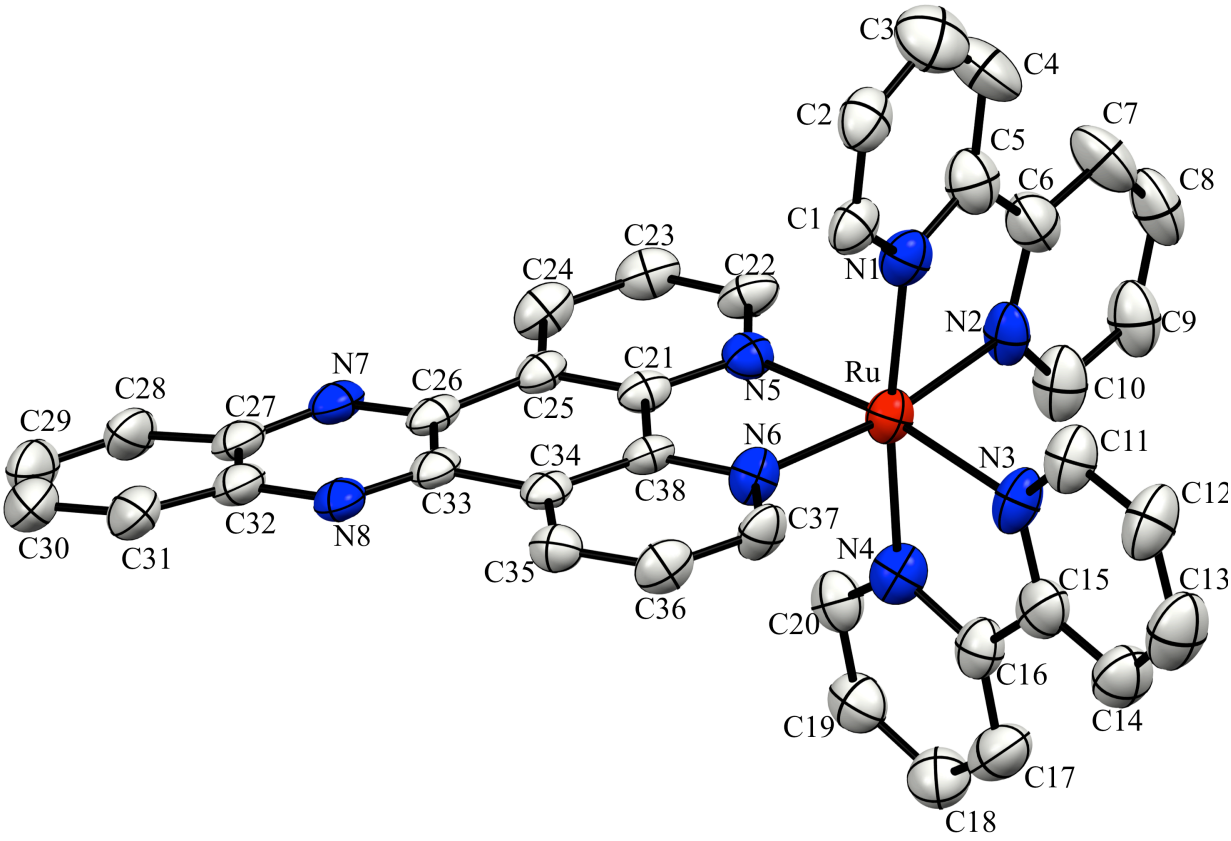

Figure S15. Ellipsoid plot of **1**. Ellipsoids are drawn at 50% probability, and hydrogen atoms are omitted for clarity. Note the crystal structure contained two crystallographically independent cations; only one is shown here.

Table S2. Selected bond lengths (Å), bond angles (°), and torsion angles (°) for **1** (B cation).

Selected Bond Lengths (Å)			
Ru-N1	2.057(8)	Ru-N2	2.055(7)
Ru-N3	2.066(7)	Ru-N4	2.065(8)
Ru-N5	2.074(7)	Ru-N6	2.072(7)
Selected Bond Angles (°)			
N1-Ru-N2	78.6(3)	N1-Ru-N3	96.6(3)
N1-Ru-N4	171.8(3)	N1-Ru-N5	90.6(3)
N1-Ru-N6	95.9(3)	N2-Ru-N3	93.2(3)
N2-Ru-N4	95.3(3)	N2-Ru-N5	93.1(3)
N2-Ru-N6	170.7(3)	N3-Ru-N4	78.2(3)
N3-Ru-N5	171.2(3)	N3-Ru-N6	94.9(3)
N4-Ru-N5	95.1(3)	N4-Ru-N6	90.8(3)
N5-Ru-N6	79.3(3)		
Selected Torsion Angles (°)			
N1-Ru-N2-C6	-3.4(7)	N2-Ru-N1-C5	4.5(6)
N1-C5-C6-N2	2.2(13)	Ru-N1-C1-C2	-177.5(7)
Ru-N2-C10-C9	177.0(7)	Ru-N1-C5-C6	-5.0(11)
Ru-N2-C6-C5	1.7(11)		
N3-Ru-N4-C16	-2.4(6)	N4-Ru-N3-C15	-3.4(7)
N3-C15-C16-N4	-4.9(12)	Ru-N3-C11-C12	176.2(8)
Ru-N4-C20-C19	172.3(7)	Ru-N3-C15-C16	2.8(10)
Ru-N4-C16-C15	4.6(10)		
N5-Ru-N6-C38	4.0(6)	N6-Ru-N5-C21	-5.3(5)
N5-C21-C38-N6	-2.5(10)	Ru-N5-C22-C23	171.0(6)
Ru-N6-C37-C36	179.4(7)	Ru-N5-C21-C38	5.8(8)
Ru-N6-C38-C21	-2.2(9)		

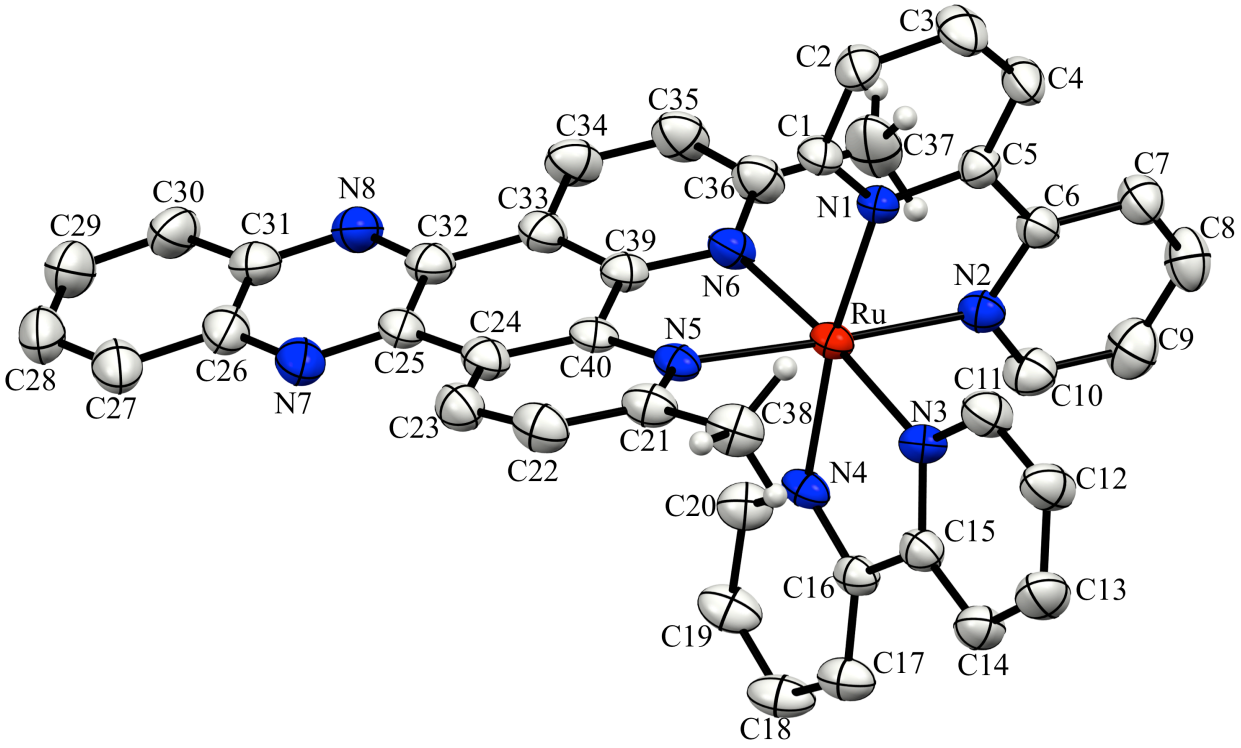

Figure S16. Ellipsoid plot of **2**. Ellipsoids are drawn at 50% probability, and hydrogen atoms are omitted for clarity. Note the crystal structure contained two crystallographically independent cations; only one is shown here.

Table S3. Selected bond lengths (Å), bond angles (°), and torsion angles (°) for **2** (A cation).

Selected Bond Lengths (Å)			
Ru-N1	2.056(4)	Ru-N2	2.065(3)
Ru-N3	2.061(4)	Ru-N4	2.073(4)
Ru-N5	2.096(4)	Ru-N6	2.112(4)
Selected Bond Angles (°)			
N1-Ru-N2	79.02(15)	N1-Ru-N3	93.76(15)
N1-Ru-N4	171.75(15)	N1-Ru-N5	98.29(14)
N1-Ru-N6	92.17(14)	N2-Ru-N3	81.33(15)
N2-Ru-N4	96.19(15)	N2-Ru-N5	177.14(14)
N2-Ru-N6	100.36(15)	N3-Ru-N4	78.80(15)
N3-Ru-N5	99.89(15)	N3-Ru-N6	174.04(14)
N4-Ru-N5	86.60(14)	N4-Ru-N6	95.31(15)
N5-Ru-N6	78.68(15)		
Selected Torsion Angles (°)			
N1-Ru-N2-C6	4.0(3)	N2-Ru-N1-C5	-4.3(3)
N1-C5-C6-N2	-0.5(6)	Ru-N1-C1-C2	175.1(4)
Ru-N2-C10-C9	-178.2(4)	Ru-N1-C5-C6	4.0(5)
Ru-N2-C6-C5	-3.1(5)		
N3-Ru-N4-C16	-0.1(3)	N4-Ru-N3-C15	-0.34(3)
N3-C15-C16-N4	-0.7(6)	Ru-N3-C11-C12	-178.2(4)
Ru-N4-C20-C19	-178.2(4)	Ru-N3-C15-C16	0.7(5)
Ru-N4-C16-C15	0.4(5)		
N5-Ru-N6-C39	-15.1(3)	N6-Ru-N5-C40	16.2(3)
N5-C40-C39-N6	1.9(6)	Ru-N5-C21-C22	-169.9(4)
Ru-N6-C36-C35	172.1(4)	Ru-N5-C40-C39	-14.9(5)
Ru-N6-C39-C40	12.1(5)		

11. References

1. J.-L. Yao, X. Gao, W. Sun, S. Shi and T.-M. Yao, *Dalton Trans.*, 2013, **42**, 5661.
2. G. Che, W. Li, Z. Kong, Z. Su, B. Chu, B. Li, Z. Zhang, Z. Hu and H. Chi, *Synthetic Commun.*, 2006, **36**, 2519.
3. E. Amouyal, A. Homsi, J.-C. Chambron and J.-P. Sauvage, *J. Chem. Soc. Dalton Trans.*, 1990, 1841.
4. S. Parkin and H. Hope, *J. Appl. Cryst*, 1998, **31**, 945.
5. APEX2, ed. Bruker-Nonius, Madison WI. USA, 2004.
6. S. Parkin, B. Moezzi and H. Hope, *J. Appl. Cryst*, 1995, **28**, 53.
7. G. M. Sheldrick, *Acta Cryst.*, 2008, **A64**, 112.
8. S. Parkin, *Acta Cryst.*, 2000, **A56**, 157.
9. *International Tables for Crystallography, Vol C: Mathematical, Physical and Chemical Tables.*, Kluwer Acedemic Publishers, Holland, 1992.
10. E. Wachter, D. K. Heidary, B. S. Howerton, S. Parkin and E. C. Glazer, *Chem. Commun.*, 2012, **48**, 9649.
11. S. R. Dalton, S. Glazier, B. Leung, S. Win, C. Megatulski and S. J. N. Burgmayer, *J. Biol. Inorg. Chem.*, 2008, **13**, 1133.
12. Y. Liu, D. B. Turner, T. N. Singh, A. M. Angeles-Boza, A. Chouai, K. R. Dunbar and C. Turro, *J. Am. Chem. Soc.*, 2009, **131**, 26.
13. R. B. Nair, B. M. Cullum and C. J. Murphy, *Inorg. Chem.*, 1997, **36**, 962.
14. A. E. Friedman, J.-C. Chambron, J.-P. Sauvage, N. J. Turro and J. K. Barton, *J. Am. Chem. Soc.*, 1990, **112**, 4960.